Published in final edited form as:
Adv Mater. 2013 May 7; 25(17): 2409–2414. doi:10.1002/adma.201204678.

Protein-protein nanoimprinting of silk fibroin films

Mark A Brenckle,
Tufts University, Department of Biomedical Engineering, 4 Colby St. Medford, MA 02155 (USA)

Dr. Hu Tao,
Tufts University, Department of Biomedical Engineering, 4 Colby St. Medford, MA 02155 (USA)

Dr. Sunghwan Kim,
Tufts University, Department of Biomedical Engineering, 4 Colby St. Medford, MA 02155 (USA)

Mark Paquette, **Prof. David L Kaplan**, and
Tufts University, Department of Biomedical Engineering, 4 Colby St. Medford, MA 02155 (USA)

Fiorenzo G Omenetto*

Abstract

Control of the interface between biological tissue and high technology materials is paramount for the development of future applications in biomedicine, especially in the case of implantable integrated devices for signal transduction.[1]-[3] Such work requires careful materials design to develop devices that can efficiently perform technological functions while retaining biocompatibility and biological integration. Silk fibroin protein from the *Bombyx mori* silkworm has come of considerable interest in this context, owing to its attractive mechanical,[4]-[7] biological, [8][9] and optical properties.[10][11] Recent work has shown adaptation of common micro- and nano-fabrication tools to silk films,[12]-[18] as well as silk protein secondary structure patterning techniques,[19] leading to biocompatible and degradable electronic and photonic devices which can simultaneously act as a carrier and stabilizer for protein pharmaceuticals and other bioactive reagents.[20]-[23] In particular, silk based nanoscale photonic devices face the challenge of sub-wavelength resolution fabrication on a soft polymeric substrate.[15][24] Previous work introduced the possibility of direct, rapid nanoimprinting in silk for the fabrication of photonic structures by leveraging the material properties of this protein.[25]

Keywords

silk; biopolymer; protein; nanoimprinting; fabrication

In this context, the glass transition temperature (T_g) of the protein is a parameter of particular relevance. In a silk film dried under ambient conditions, the water retained by the film acts as a plasticizer, significantly lowering the glass transition from 178°C to ~78°C.[26] The actual T_g depends inversely on the water content and can be modeled as a function of the fractions of silk and water in the dried construct.[27] In imprinting, the application of heat and pressure to a silk fibroin film layered on a hard mask rapidly pushes the film above T_g, causing it to transition from a glassy state to a liquid-like rubber, allowing reflow of polymer on the nanoscale.[25]

*Prof. F. G. Omenetto, Tufts University, Department of Biomedical Engineering, 4 Colby St. Medford, MA 02155 (USA), Fiorenzo.Omenetto@tufts.edu.

In this work, we expand upon this technique by exchanging the conventionally fabricated hard silicon or glass masters with a second silk fibroin film, in a process we term protein-protein imprinting (or PiP for short). This is accomplished by control of the water content and beta-sheet crystallinity of each of the two films. Though the heat and pressure application are similar to the previous technique, using a dry, crystallized fibroin master and a wet, uncrystallized "blank" film allows for reflow of the template film only and limits the adhesion between the two layers for easy release. As an improvement to the current technique, this method significantly increases throughput, reduces dependence on the hard mask, and, additionally, allows for direct conformal imprinting on curved surfaces due to the flexibility of the nanoimprinted silk master.

Nanoimprint lithography on nonplanar surfaces has been investigated recently for applications in spectroscopy,[28] superhydrophobic structures,[29] and microlens arrays,[30][31] and has shown resolution on the order of ~100 nm. Here, a wide variety of approaches have been attempted, ranging from nanoimprint lithography with flexible materials to chemical vapor deposition assisted methods. Most of these currently available techniques suffer from complex procedures or destruction of the imprint master.[32]-[34] The required photoresists and imprinted materials are often not biocompatible, limiting their use in biomedical applications.[34] Furthermore, most of those processes are relatively time consuming, with a required imprinting duration ranging from a few minutes to several hours. For example, a common conformal printing technique using thin poly(dimethylsiloxane) (PDMS) membranes usually requires ~5 min imprint times for a resolution of ~500 nm, and lacks long term repeatability due to master deformation after repeated heating for the long imprinting time.[32] Further, none of these prior approaches provides facile modes to incorporate bioactive components with retention of function, a feature that permits broader utility in medical devices and other domains.

For the application of PiP to nonplanar surfaces we demonstrate resolution on the order of currently available nonplanar imprint technologies, with higher throughput and fewer concerns about master durability. In addition, due to the biocompatibility of silk, nonplanar PiP can be used to apply nanophotonic structures to curved biological surfaces.[1][3] Together, this approach provides a versatile and simple fabrication method for biointegrated silk devices, further expanding the utility of silk fibroin as a bridge between high technology and biomedical applications.

Method and Mechanism

The PiP process is shown in Figure 1a. A patterned silk master, shown in yellow, was placed underneath the film to be protein imprinted, shown in blue, on a smooth polished Ni surface (for uniform thermal distribution) heated to 120°C. About 50 Psi of pressure was applied to the top and held for between 5 and 60 seconds, during which reflow occurred. This produced the inverse pattern in the blank film, as shown in the scanning electron microscope (SEM) images. If crystallization occurs in the imprinted film, this new film could be utilized as a master for a subsequent generation, which would then have the original pattern, as shown in step two. Such a methodology could lead to multiplexing the production of films (for instance two imprints per generation would yield 4 positive and 8 negative imprints of the master in only three generations).

Indeed, crystallization of the imprinted films does take place, as is shown in Figure 1c. Here, Fourier-transform infrared (FTIR) spectra were taken for heated films at 5-second intervals, and beta-sheet content of the films was quantified using previously established curve-fitting procedures.[35]-[37] At 120°C and ~50 Psi, the kinetics of crystallization occurred rapidly, with the films reaching a crystalline plateau after only 15 seconds of pressure. This plateau

was found to be equivalent, if not higher, in crystalline content to conventional silk film annealing treatments such as exposure to methanol. Additionally, the hydration state of the films was monitored using Thermal Gravimetric Analysis (TGA), in a similar procedure. Films dried under ambient conditions were found to have ~10.4% residual water, which rapidly decreased to ~7% as the crystallinity increased, as shown in Fig. 1c. This corresponds to little change in the T_g of the plasticized film, with a glass transition close to 80°C in all cases.

The adhesion of the two layers after imprinting is essential to the success of the process, as difficulty in separating the two films could cause damage to either nanoscale pattern, decreasing yield. Investigation of the inter-layer adhesion was examined, by performing tensile testing (Instron 3360, Instron Inc., Norwood, MA) both for untreated films, and films crystallized via the PiP method. The figure shows a 6-fold decrease in interfacial strength, to a value of less than 500 kPa, indicating easy separation of the two layers after PiP, because of the crystallization of the films. This property is advantageous, as both high and low adhesion strengths are possible in the same material through the control of the thermal transition, thus enabling imprinting.

Additionally, the data indicate that the crystallization plateau is responsible for locking the imprinted pattern into place, as the T_g does not change appreciably with the modest (~3%) reduction in water content seen here.[27] The kinetics of crystallization, and thus reflow, occurs rapidly, which means PiP imprints may be possible on an even shorter timescale. This confirms that it should be possible to directly imprint subsequent generations utilizing imprinted owing to the high degree of crystallinity imparted by the process.

Characterization

The PiP mechanism suggests the possibility of multi-generation imprinting, which was confirmed by evaluating the pattern quality (i.e. resolution) with subsequent imprinted generations. For this, electron beam lithography written periodic photonic crystal structures of 100 nm tall, 200 nm diameter Cr pillars on Si - which serves as the original (non-silk) master and a baseline for imprinting quality comparison - was utilized, with lattice constants varying from 200-700 nm. The optical response under darkfield illumination (Olympus IX71, Center Valley, PA) as well as the surface profile measured via atomic force microscopy (AFM)(Veeco Dimension 3100, Plainview, NY) have been collected, as shown on the right hand side of Figure 2d. The mean cross section of the image is shown on the left. This master was utilized to create an inverse silk master through the previous rapid nanoimprinting technique (Figure 2c). The results show good spatial and optical fidelity, with a slight reduction in pattern depth (57 nm vs. 80 nm), accompanied by sharper features at the extremes.

The silk master was then utilized in PiP to create a first generation imprint (Figure 2b), which in turn imprinted the second generation, which then produced the third (Figure 2a). The results of these imprints show a modest reduction in reproduction of the nanoscale features with each subsequent generation, marked by rounding of the sharp edges of the features. No further decrease in feature depth was seen, and more importantly, no appreciable change in optical response was noted. This indicates that in addition to strong replication of vertical features, no large-scale distortion in the lattice constant occurred during imprinting. Some rounding of edges at the feature tips was noted, but is likely due to the lack of pressure optimization. Based on this the possibility of at least three generations of imprints via the PiP method seems to be a reasonable assertion. Given this, the number of possible samples becomes N^2+1 negative and $N^2 + N^3$ positive imprints, where N is the number of imprints per generation. As further generations beyond this are produced, the

quality will degrade, eventually affecting the macroscale properties and efficacy of the imprinted patterns.

The exploration of the PiP mechanism above also indicates the possibility of optimization of the PiP procedure for specific applications by altering the temperature and time used for imprinting. This was assessed via a similar experiment within a broad range of these two primary imprinting parameters. Here, a silk master of a similar lattice, with optical response shown in Figure 3c-e, was utilized to imprint a single generation, which was then investigated via AFM. This master however, was produced to have an initial hole depth of ~500 nm, with a similar diameter of 200 nm and lattice constants varying from 200-700 nm. The results of the imprinting process are shown in Figure 3a. Once again, a reduction in hole depth was seen with the first imprint, and rounding of the features was noted, as expected given consistency in the pressure parameter. Imprints were made at temperatures between 70 and 120°C for times between 5 and 60 seconds.

An interpolated contour plot of the results is shown in Figure 3b. The results show a maximum depth of above 400 nm, reached at ~20 seconds for 120°C. and ~30 seconds near 100°C. the depth then rapidly decreased, with no imprints made below 80°C. This response makes sense given the PiP mechanism, where no reflow occurs below T_g. The kinetics of crystallization, determined by the temperature used, would be slower at lower temperatures leading to the slower reflow response noted here.[38] This broad parameter space for imprinting allows the PiP parameters to be tailored to the application.

The same master was used though the course of this experiment, and was analyzed before and after use. The results are shown in Figure 3c-e, with 3c and 3e representing the same master before and after being used for 18 imprints, and 3d showing a characteristic image of one of those imprints. As before, the imprint showed rounding of the features, with little measured variation in depth. The master, however, shows little to no change after 18 uses, specifically on the nanoscale, as the cross sections show. The consistent colorimetric responses show again a lack of distortion in the horizontal, across the entire imprinted region. This indicates that 18 imprints is a reasonable expectation for each generation, which would yield a maximum of $N^2+1 = 325$ negative and $N^2 + N^3 = 6,156$ positive imprints from a single use of the original master. With each of these imprints occurring in as little as 20 seconds, and accounting for the possibility of multiplexing (Figure 1a(2)), PiP is a viable option for high-throughput nanofabrication on silk fibroin films.

Conformal Imprinting and Extensions

In addition to increasing throughput, the relative flexibility of the silk fibroin masters as compared to a hard silicon or metal mask was leveraged to directly achieve conformal imprinting. The modified scheme for this method is shown in Figure 4a, and is nearly identical to the previous method, with the inclusion of a machined aluminum tool for homogenous pressure distribution normal to the imprinted surface. PiP was used to imprint directly on a plano-convex lens with diameter of 15 mm and radius of curvature of 9.8 mm, whose surface was coated with a thin layer of silk (Figure 4b). After PiP at 120°C for 60 sec, the surface was evaluated with AFM (Figure 4d,e). The results showed good reproduction of the master pattern on the microscale of features on the order of 100 nm, which is comparable to currently available options,[32]-[34] while the optical response (Figure 4b, inset) shows coverage over the entire curved lens surface. The combination of this technique with previously reported silk transfer techniques for arbitrary surface transfer [39][1][2] can yield conformal contact on curved tissue surfaces, as is demonstrated in Figure 4c. Here, the film was removed from the lens and transferred and adhered to the skin. By this method, PiP can be used to manufacture molded curvilinear silk protein based sensing devices that could

integrate with the human body. The possibility of a skin-skin mounted sensor fabricated using PiP was explored as a proof of concept demonstration by monitoring the shift in the colorimetric response of the device with the addition of a thin coat of ethanol (Figure 4c, inset).

Conclusions

PiP is introduced as a rapid, high-throughput method for the fabrication of nanoscale structures in silk films. The possibility of at least 3 generations of imprints with at least 18 imprints per generation was demonstrated, making this a truly high throughput technique. Application to conformal surfaces is possible with minor adjustments to the system, at resolutions comparable to other currently available non-planar nanoimprint lithography techniques. The addition of PiP to the silk materials fabrication toolbox opens new avenues for biocompatible device fabrication, which will further expand the utility of silk as a bridge between high technology and biomedical applications.

Experimental

Silk Processing—Aqueous silk solution was produced by regeneration from *Bombyx mori* cocoons according to established procedures.[5] Briefly, the cocoons were boiled for 30 min in sodium carbonate (0.2M) to remove sericin, glue like protein holding the cocoon together. The fibers were dried overnight, and then dissolved in lithium bromide (9M). Dialysis against Milli-Q for ~72h yielded a roughly 6% aqueous solution of silk fibroin. All casting work was carried out on a PDMS surface or directly on a patterned silicon master. The films were dried at ambient conditions (~25°C, ~40% RH) and resulted in films that were ~100 μm thick.

Silk masters were produced using these films, and applying the existing silk nanoimprint lithography technique,[10][25], by heating to ~120°C for 60 sec against a metal master. Heat treatment has been previously reported to be able to tune the β-sheet crystallinity of silk fibroin without causing the microscale fractures that can occur with methanol treatment, and were used to crystallize the master in this work.

FTIR spectroscopy—FTIR scans were taken on a (Jasco FTIR 6200, Easton, MD) spectrometer with attached ATR detector. A total of 64 scans at a resolution of 4.0 cm^{-1} were co-added to produce spectra ranging from 400 – 4000 cm^{-1}. A cosine apodization was simultaneously applied by the software. From these scans, the amide III region (1200 – 1350 cm^{-1}) was selected for its sensitivity to protein secondary structure and lack of sensitive to water content. Amide III curves were normalized and baseline corrected, and then fit to 12 Gaussian curves, according to the work of Wei et al.[37] Bands corresponding to β-sheet secondary structure motifs were then added to give a relative value for the β-sheet crystalline content of the films.

Thermal gravimetric analysis (TGA)—Water content of the silk films was assessed through TGA (TA Instruments Q500, New Castle, DE). Films were heated to 200°C at a rate of 10°C min^{-1} with a constant mass measurement. All of the mass lost during this procedure was determined to be water evaporation, according to published results. All water is removed by 187°C, and total water removal is independent of heating rate for silk fibroin films.[26]

Tensile Testing—Tensile testing (Instron 3360, Instron Inc.) of the interface between the two films was performed for mode 2 failure via a conventional lap shear configuration. This process was similar to ASTM D3163, with modified geometry due to specimen limitations

Conformal-PiP Die Fabrication—An aluminum piece was machined on a lathe to the inverse specifications of the surface to be imprinted, in order to ensure pressure was normal to the surface in all locations. Aluminum was selected as the material for this piece due to its high thermal conductivity (~230 W m^{-1} K^{-1}), to ensure that the heat transfer properties of the system were minimally affected.

Silk film transfer—Silk films were transferred onto skin via a previously established transfer procedure.[39] Briefly, the side of the film to be attached was exposed to a high (~90%) relative humidity environment for a few seconds to partially solubilize the film. The film was then applied to the transfer surface with light pressure and allowed to dry, thereby attaching it to the surface of the skin.

Acknowledgments

This material is based upon work supported by DARPA-MTO and the NIH. ((Supporting Information is available online from Wiley InterScience or from the author)).

References

1. Kim D-H, Lu N, Ma R, Kim Y-S, Kim R-H, Wang S, Wu J, Won SM, Tao H, Islam A, Yu KJ, Kim T, Chowdhury R, Ying M, Xu L, Li M, Chung H-J, Keum H, McCormick M, Liu P, Zhang Y-W, Omenetto FG, Huang Y, Coleman T, Rogers Ja. Science. 2011; 333:838–43. [PubMed: 21836009]
2. Kim D, Viventi J, Amsden JJ, Xiao J, Vigeland L, Kim Y-S, Blanco Ja, Panilaitis B, Frechette ES, Contreras D, Kaplan DL, Omenetto FG, Huang Y, Hwang K-C, Zakin MR, Litt B, Rogers Ja. Nature Materials. 2010; 9:511–517.
3. Viventi J, Kim D-H, Vigeland L, Frechette ES, Blanco Ja, Kim Y-S, Avrin AE, Tiruvadi VR, Hwang S-W, Vanleer AC, Wulsin DF, Davis K, Gelber CE, Palmer L, Van der Spiegel J, Wu J, Xiao J, Huang Y, Contreras D, Rogers Ja, Litt B. Nature Neuroscience. 2011; 14:1599–605.
4. Lawrence BD, Omenetto F, Chui K, Kaplan DL. Journal of Materials Science. 2008; 43:6967–6985.
5. Sofia S, McCarthy MB, Gronowicz G, Kaplan DL. Journal of Biomedical Materials Research. 2001; 54:139–48. [PubMed: 11077413]
6. Meinel L, Betz O, Fajardo R, Hofmann S, Nazarian a, Cory E, Hilbe M, McCool J, Langer R, Vunjak-Novakovic G, Merkle HP, Rechenberg B, Kaplan DL, Kirker-Head C. Bone. 2006; 39:922–31. [PubMed: 16757219]
7. Jin H-J, Fridrikh SV, Rutledge GC, Kaplan DL. Biomacromolecules. 2002; 3:1233–9. [PubMed: 12425660]
8. Santin M, Motta a, Freddi G, Cannas M. Journal of Biomedical Materials Research. 1999; 46:382–9. [PubMed: 10397996]
9. Pritchard EM, Szybala C, Boison D, Kaplan DL. Journal of Controlled Release : Official Journal of the Controlled Release Society. 2010; 144:159–67. [PubMed: 20138938]
10. Perry H, Gopinath A, Kaplan DL, Dal Negro L, Omenetto FG. Advanced Materials. 2008; 20:3070–3072.
11. Lawrence BD, Cronin-Golomb M, Georgakoudi I, Kaplan DL, Omenetto FG. Biomacromolecules. 2008; 9:1214–20. [PubMed: 18370418]
12. White RD, Gray C, Mandelup E, Amsden JJ, Kaplan DL, Omenetto FG. Journal of Micromechanics and Microengineering. 2011; 21:115014.
13. Tsioris K, Tao H, Liu M, Hopwood JA, Kaplan DL, Averitt RD, Omenetto FG. Advanced Materials. 2011; 23:2015–9. [PubMed: 21445939]
14. Tsioris K, Tilburey GE, Murphy AR, Domachuk P, Kaplan DL, Omenetto FG. Advanced Functional Materials. 2010; 20:1083–1089.
15. Mondia JP, Amsden JJ, Lin D, Negro LD, Kaplan DL, Omenetto FG. Advanced Materials. 2010; 22:4596–9. [PubMed: 20859936]

16. Tao H, Chieffo LR, Brenckle MA, Siebert SM, Liu M, Strikwerda AC, Fan K, Kaplan DL, Zhang X, Averitt RD, Omenetto FG. Advanced Materials. 2011; 23:3197–201. [PubMed: 21638342]
17. Young SL, Gupta M, Hanske C, Fery A, Scheibel T, Tsukruk VV. Biomacromolecules. 2012; 13:3189–99. [PubMed: 22947370]
18. Galeotti F, Andicsova A, Yunus S, Botta C. Soft Matter. 2012; 8:4815.
19. Gupta MK, Singamaneni S, McConney M, Drummy LF, Naik RR, Tsukruk VV. Advanced Materials. 2010; 22:115–119. [PubMed: 20217709]
20. Zhang J, Pritchard E, Hu X, Valentin T, Panilaitis B, Omenetto FG, Kaplan DL. Proceedings of the National Academy of Sciences of the United States of America. 2012
21. Tsioris K, Raja WK, Pritchard EM, Panilaitis B, Kaplan DL, Omenetto FG. Advanced Functional Materials. 2012; 22:330–335.
22. Tao H, Kaplan DL, Omenetto FG. Advanced Materials (Deerfield Beach, Fla). 2012; 24:2824–37.
23. Domachuk P, Perry H, Amsden JJ, Kaplan DL, Omenetto FG. Applied Physics Letters. 2009; 95:253702. [PubMed: 20087427]
24. Lee SY, Amsden JJ, Boriskina SV, Gopinath A, Mitropolous A, Kaplan DL, Omenetto FG, Dal Negro L. Proceedings of the National Academy of Sciences of the United States of America. 2010; 107:12086–90. [PubMed: 20566892]
25. Amsden JJ, Domachuk P, Gopinath A, White RD, Negro LD, Kaplan DL, Omenetto FG. Advanced Materials. 2010; 22:1746–9. [PubMed: 20496408]
26. Hu X, Kaplan D, Cebe P. Thermochimica Acta. 2007; 461:137–144.
27. Agarwal N, Hoagland DA, Farris RJ. Journal of Applied Polymer Science. 1998; 63:401–410.
28. Xie Y, Lu Z, Li F. Optics Express. 2003; 11:992–5. [PubMed: 19465961]
29. Mishchenko L, Hatton B, Bahadur V, Taylor JA, Krupenkin T, Aizenberg J. ACS Nano. 2010; 4:7699–7707. [PubMed: 21062048]
30. Hoshino K, Mura F, Shimoyama I. IEEE Conference on Micro-electro Mechanical Systems. 1999:429–434.
31. Jacobs HO, Tao AR, Schwartz A, Gracias DH, Whitesides GM. Science. 2002; 296:323–5. [PubMed: 11951039]
32. Choi WM, Park OO. Nanotechnology. 2004; 15:1767–1770.
33. Mukherjee R, Patil GK, Sharma A. Industrial Engineering Chemical Research. 2009:8812–8818.
34. Farshchian B, Amirsadeghi A, Hurst SM, Wu J, Lee J, Park S. Microelectronic Engineering. 2011; 88:3287–3292.
35. Lórenz-Fonfría, Va; Padrós, E. Spectrochimica Acta Part A, Molecular and Biomolecular Spectroscopy. 2004; 60:2703–10.
36. Hu X, Kaplan D, Cebe P. Macromolecules. 2006; 39:6161–6170.
37. Wei Q-N, Huang A-M, Ma L, Huang Z, Huang X, Qiang P-P, Gong Z-P, Zhang L. Journal of Applied Polymer Science. 2012; 125:E477–E484.
38. Hu X, Shmelev K, Sun L, Gil E-S, Park S-H, Cebe P, Kaplan DL. Biomacromolecules. 2011; 12:1686–96. [PubMed: 21425769]
39. Tao H, Brenckle MA, Yang M, Zhang J, Liu M, Siebert SM, Averitt RD, Mannoor MS, McAlpine MC, Rogers Ja, Kaplan DL, Omenetto FG. Advanced Materials. 2012; 24:1067–72. [PubMed: 22266768]

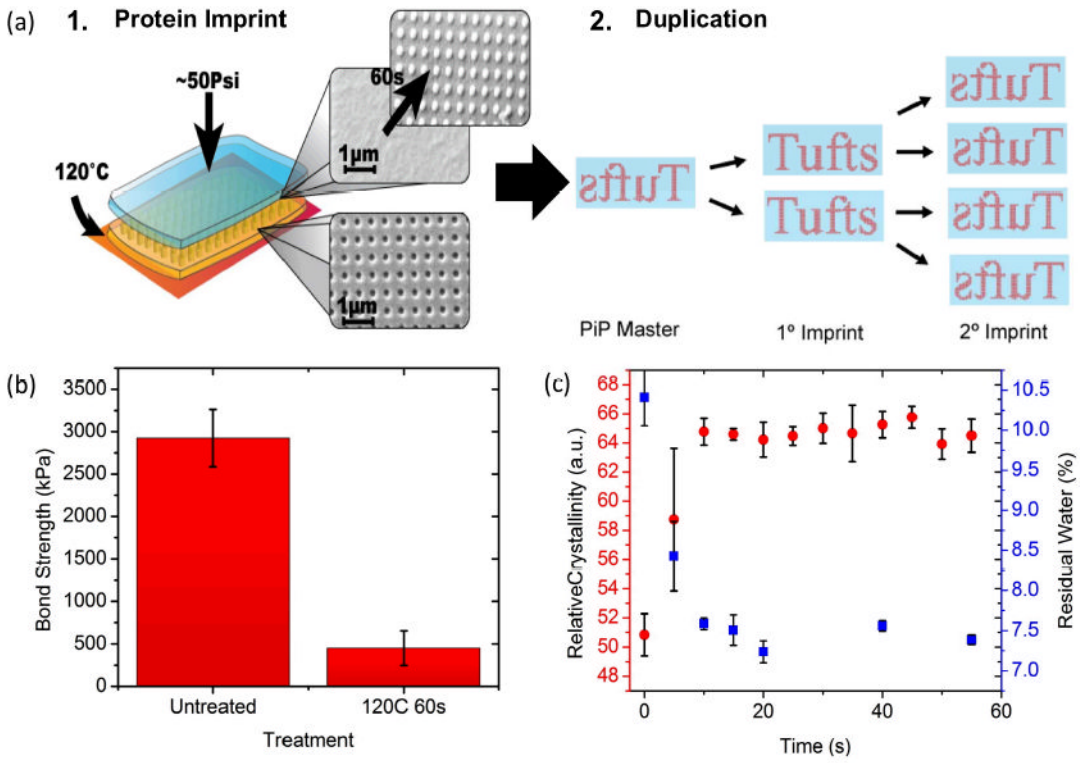

Figure 1. Schematics of the PiP process, and replication mechanism

(a) Each imprint was made by layering an untreated, unpatterned (blue) film on top of a crystallized, patterned silk fibroin master (yellow). These samples were placed on a heated substrate at 120°C for 60 seconds, with ~50 Psi pressure. Reflow of the untreated films, to generate an inverse pattern in the untreated film (SEM micrographs, inset) complete the pattern transfer. Duplication can be carried out by using each generation to imprint the next, as shown with red representing patterns on the blue films, making the technique truly high-throughput. **(b)** Lap shear bond strength for two overlapped, PiP- pressed films of untreated and 120°C 60 seconds pretreatment. A 6-fold decrease in bond strength was seen with the crystallized films. **(c)** Crystallization rates (red points) as measured through quantified FTIR (see methods), and residual water content (blue points), as quantified through TGA, for films throughout the PiP process. A crystallized plateau was reached after 15 seconds of pressing. Water loss follows the inverse pattern of crystallization, rapidly decreasing from ~10.5% to ~7.25% with treatment.

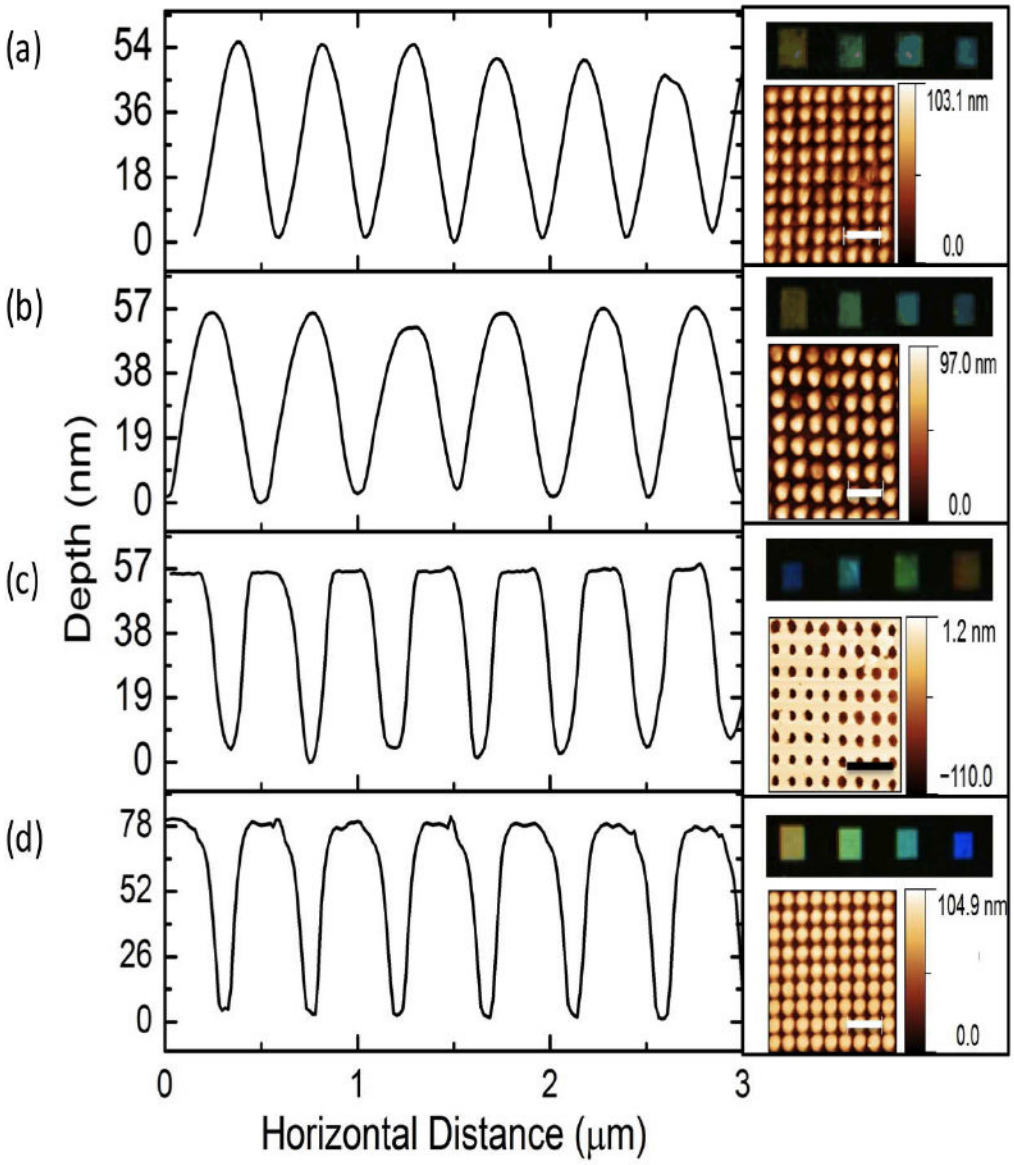

Figure 2.

Characterization of multi-generation PiP imprint, showing mean AFM cross section, AFM topology, and darkfield optical response of 200 nm diameter nanopillar lattice. Scale bars 1 μm. **(a)** Third generation imprint. **(b)** First generation PiP imprint. **(c)** Silk master generated through nanoimprint lithography. **(d)** Silicon master fabricated through electron beam lithography. Results show consistent replication of dimensions, with some rounding of feature “tips”, and consistent optical response, indicating strong large scale reproduction of both horizontal and vertical dimensions.

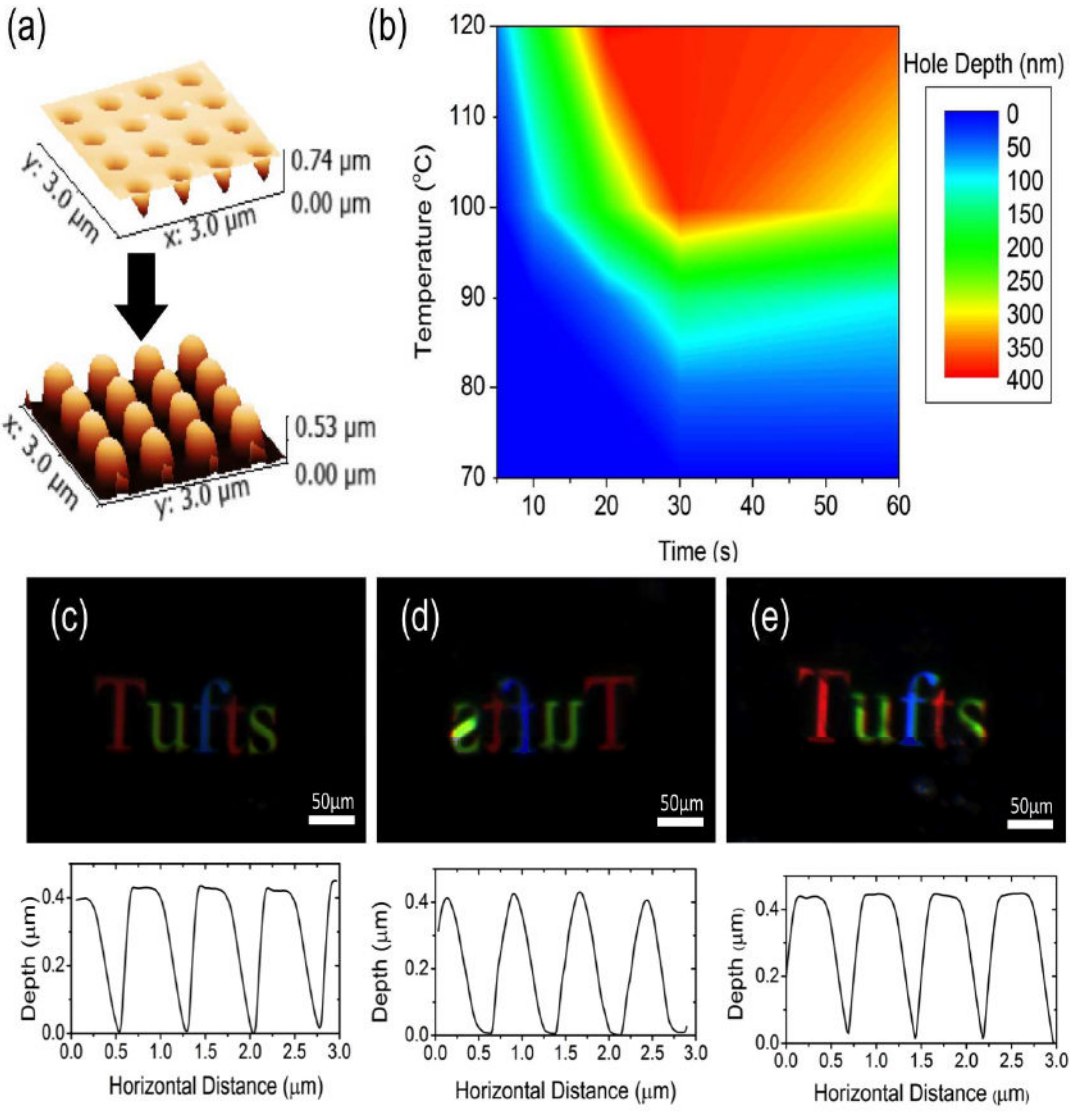

Figure 3. Characterization of PiP parameter space

(a) Three dimensional image of AFM measured topography of PiP imprint process for parameter space characterization, showing the master on top, and a representative image of an imprint below. **(b)** Interpolated contour plot of imprint quality as measured by hole depth over PiP parameter space. Differences in kinetics with temperature are clearly seen, with broad possible parameter space for good replication. No response seen below 80°C, corresponding to the expected glass transition of the polymer. **(c)** Darkfield optical response and AFM cross-section of silk master, indicating good large-scale replication, and consistent lattice constant **(e)** Characteristic optical response and AFM section of PiP imprints. Imprinted at 110°C for 30 seconds, indicating good large scale replication, and consistent lattice constant **(e)** Darkfield optical response and AFM cross-section of silk master after 18 uses, corresponding well to the results of Figures 3b, and 3c. Little horizontal distortion seen in pattern.

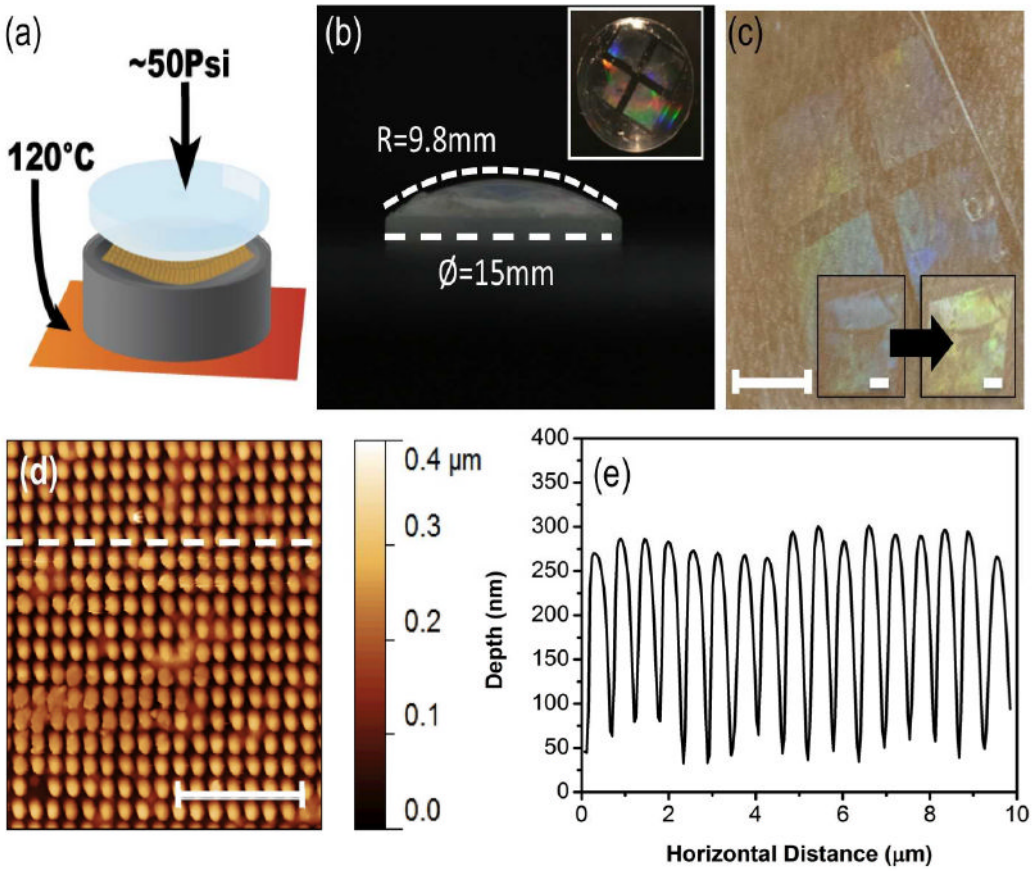

Figure 4. Conformal PiP and surface transfer

(a) Modification to the PiP process for conformal imprint, showing the addition of non-planar aluminum tool (gray) for homogenous pressure application normal to the imprinting surface. **(b)** Lens characteristics, 9.8 mm radius of curvature, 15 mm diameter. Inset: Imprinted lens, using optimized PiP method. **(c)** Transfer of film imprinted on lens to skin as example curved biological surface (scale bar 4 mm). Inset: change in colorimetric response of the imprinted film with the addition of ethanol to the surface (scale bars 1 mm). **(d)** AFM topology of conformal PiP imprint, with dashed line corresponding to cross-section Scale bar 5μm. **(e)** AFM cross-section of conformal imprint, showing good pattern replication across all dimensions.